
Doctoral Dissertations

Student Theses and Dissertations

1970

Absolute excitation cross sections of He⁺ in 20-100 keV He⁺-He collisions using energy-loss spectrometry

Donald Roy Schoonover

Follow this and additional works at: https://scholarsmine.mst.edu/doctoral_dissertations



Part of the [Physics Commons](#)

Department: Physics

Recommended Citation

Schoonover, Donald Roy, "Absolute excitation cross sections of He⁺ in 20-100 keV He⁺-He collisions using energy-loss spectrometry" (1970). *Doctoral Dissertations*. 2121.

https://scholarsmine.mst.edu/doctoral_dissertations/2121

This thesis is brought to you by Scholars' Mine, a service of the Missouri S&T Library and Learning Resources. This work is protected by U. S. Copyright Law. Unauthorized use including reproduction for redistribution requires the permission of the copyright holder. For more information, please contact scholarsmine@mst.edu.

ABSOLUTE EXCITATION CROSS SECTIONS OF He^+ IN
20-100 keV He^+ -He COLLISIONS USING
ENERGY-LOSS SPECTROMETRY

by

DONALD ROY SCHOONOVER, 1939-

A DISSERTATION

Presented to the Faculty of the Graduate School of the
UNIVERSITY OF MISSOURI - ROLLA

In Partial Fulfillment of the Requirements for the Degree
DOCTOR OF PHILOSOPHY

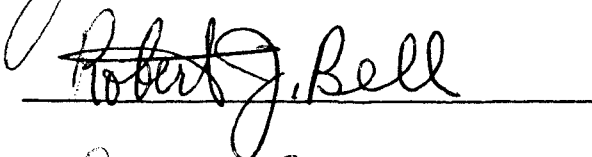
in

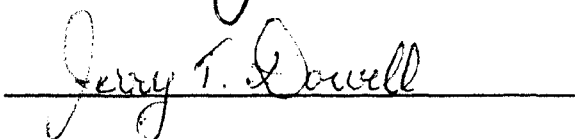
PHYSICS

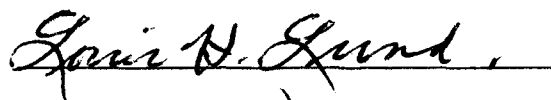
1970

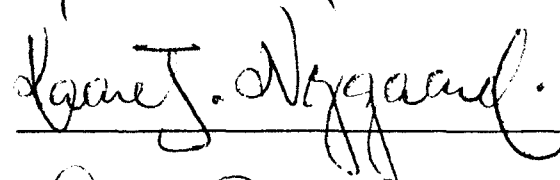


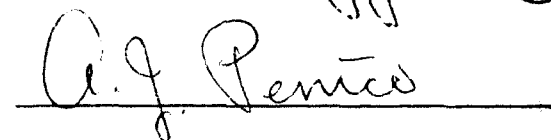
Advisor











PUBLICATION THESIS OPTION

This thesis has been prepared in the style utilized by the Physical Review. Pages 1 - 24 will be submitted for publication in that journal. Appendices A, B, and C have been added for purposes normal to thesis writing.

ABSTRACT

Application of positive-ion energy-loss spectrometry has been extended to include experimental determination of absolute excitation cross sections of ground state helium ions. Helium ion-atom collisions were studied for impact energies ranging between 20-100 keV, in 10 keV intervals. The data were taken with an apparatus resolution between 0.6-0.8 eV FWHM. Cross sections for transitions from ground state to the second and third principal quantum levels of the ion plotted as a function of impact energy were still rapidly increasing at 100 keV. The cross sections at this energy were $1.64(+0.28) \times 10^{-18} \text{ cm}^2$ for $\text{He}^+(1^2s_{1/2}) \rightarrow \text{He}^+(n=2)$ and $3.46(+0.45) \times 10^{-19} \text{ cm}^2$ for $\text{He}^+(1^2s_{1/2}) \rightarrow \text{He}^+(n=3)$.

ACKNOWLEDGMENTS

With gratitude I acknowledge indebtedness to my thesis advisor, Dr. John T. Park, without whose fine example of dynamism I might not otherwise have summoned sufficient motivation to complete such an arduous task.

Special thanks are also due to Dr. William R. Snow for his noteworthy suggestions, to George York for his technical assistance which was indispensable, to Victor Pol and Eugene Aufdembrink for their assistance with the apparatus, to Dr. R. H. McFarland for some useful literature references, and to other members of the technical staff for their helpful assistance.

Last, but certainly not least, I would like to express appreciation to my wife, Karen, and my son, Donald, whose sacrifice have been greater than my own, and to Beverly St. John for typing the manuscript.

I also appreciate the financial support received through the National Defense Education Act and from the National Science Foundation.

TABLE OF CONTENTS

	Page
ABSTRACT.....	ii
ACKNOWLEDGMENTS.....	iii
LIST OF FIGURES.....	v
LIST OF SYMBOLS.....	vii
I. INTRODUCTION.....	1
II. ANALYSIS OF TRANSITIONS IN PROJECTILE.....	3
III. DESCRIPTION OF APPARATUS AND METHOD OF OPERATION.....	9
IV. DATA.....	16
V. DISCUSSION.....	22
VI. APPENDICES.....	25
A. Theory of Positive-Ion Energy-Loss Spectrometry.....	25
1. Charge-Changing Interactions.....	35
2. Transitions in Target.....	40
B. Least-Squares Fitting of Experimental Data.....	47
C. Apparatus Modifications.....	51
VII. BIBLIOGRAPHY.....	55
VIII. VITA.....	58

LIST OF FIGURES

Figures	Page
1. Simplified partial beam model for projectile transitions.....	5
2. Schematic diagram of UMR acceleration-deceleration positive-ion energy-loss spectrometer.....	10
3. Energy loss traces (a) without target gas, and (b) with target gas.....	13
4. Energy level diagram of He^+ . (Data taken from C. E. Moore, <u>Atomic Energy Levels</u> , Nat. Bur. of Standards circular 467, June 15, 1949.).....	17
5. Absolute $\text{He}^+(1^2s_{\frac{1}{2}}) \rightarrow \text{He}^+(n = 2)$ ionic transition cross section as a function of impact energy (with He).....	20
6. Absolute $\text{He}^+(1^2s_{\frac{1}{2}}) \rightarrow \text{He}^+(n = 3)$ ionic transition cross section as a function of impact energy (with He).....	21
A1. Representative partial beam generation and loss contributions in scattering region; energy distributions of composite beams l_0 and l_2 not observed.	29
A2. Simplified composite beam model for charge-changing interactions.....	36
A3. Simplified partial beam model for target transitions.....	41
A4. Simplified partial beam model for two coincident singly-scattered beams.....	43

Figures	Page
A5. Simplified partial beam model for coincident singly-scattered and doubly-scattered beams.....	45

LIST OF SYMBOLS

a	least-squares constant
a_c	least-squares constant
a_o	1st Bohr radius of hydrogen atom
A	cross-sectional area of beam
b	least-squares constant
c	least-squares constant
e	fundamental electronic charge
I_j	(see p. 28 for definition of subscripted current symbols)
k	number of data samples
l	scattering length
m	mass of projectile
n	target particle number density
n_{eff}	effective beam particle number density
n_s	beam particle number density
N_L	Loschmidt's number
p	target gas pressure
p_o	reduced pressure
R	energy loss spectrum
s	standard deviation
T	temperature ($^{\circ}K$)
v	projectile velocity
v_s	partial beam projectile velocity
V	accelerating potential
V_o	offset voltage

V_s	equivalent accelerating potential of partial beam energy
x	displacement along collision path
y	ratio of $(I_{1p})_f$ to $(I_{10})_f$
z	$\ln[(I_{10})_f/(I_{10})_i]$
α	relative detectable singly-charged composite beam current
α_a	relative detectable singly-scattered partial beam current
β	$\sigma n \ell$
Δ	least squares function
ϵ	relative standard deviation
ζ	relative change in total loss cross section due to excitation of projectile
θ	laboratory scattering angle
λ	change in total loss cross section due to excitation of projectile
ξ	energy loss variable
σ	cross section
σ_a	typical target transition cross section
σ_b	typical target transition cross section
σ_c	total charge-changing cross section
σ_d	typical target transition cross section
σ_i	ionization cross section
σ_j	total incident beam loss cross section minus σ_c

σ_j'	σ_j minus the designated cross section
σ_ℓ	stripping cross section
σ_p	typical projectile transition cross section
σ_{jk}	cross section for transition $I_j \rightarrow I_k$
Φ	apparatus resolution function
Ω	solid angle
ΔE	collisional energy loss
ΔV	variation in offset voltage
$\Delta\xi_o$	energy-loss interval corresponding to elastically transmitted incident beam
$\Delta\xi_p$	energy-loss interval corresponding to σ_p -transition
$\Delta\Omega$	apparatus acceptance solid angle
$\sigma(a_i b_j / c_k d_\ell)$	(see p. 30 for definition)

Absolute Excitation Cross Sections of He^+ in
20-100 keV He^+ -He Collisions Using
Energy-Loss Spectrometry

I. INTRODUCTION

The technique of energy-loss spectrometry is rapidly becoming a major tool for studying elementary collision processes. In electron spectrometry, electron exchange and target transitions can be studied. In positive-ion energy-loss spectrometry, excitation of the projectile ion can also occur. Relative velocity of approach (rather than impact energy) is the primary parameter considered when making approximations in theoretical calculations.¹ Therefore, since positive ions are considerably more massive than electrons, the impact energy remains above the inelastic thresholds down to much lower velocities of approach, providing more strenuous tests for acceptable approximations.

Positive-ion energy-loss spectrometry² has recently been applied to proton impact investigation of a monatomic species (helium)³ and to a diatomic species (nitrogen).⁴ A transition has been observed by others⁵ in He^+ -He collisions which was attributed to excitation of the incident ion while the target atom remained in its ground state. The resolution, however, was not sufficient to permit accurate determination

of the cross section. Previously, the modulated crossed-beam technique was the only method available for studying excitation cross sections in a chemically unstable atomic system such as He^+ . The only studies on He^+ utilizing this technique have been with electron projectiles.⁶

The measured He^+ -He impact cross sections for excitation transitions in He^+ are needed for diagnostic evaluations in certain applications, such as controlled thermonuclear research, and in various astrophysical and cosmological phenomena. In the latter, the observation of He^+ spectral lines has indicated the presence of this ion in the ionosphere,⁷ as a solar wind component,⁸ in the ultra-violet and soft x-ray spectra of the sun,⁹ in the recombination-cascade spectrum of solar flares,¹⁰ in stellar spectra,¹¹ and in the visible and ultra-violet spectra of quasars.¹²

The resolution of the UMR positive-ion energy-loss spectrometer has recently been sufficiently improved to permit the study of ionic excitation transitions. The absolute excitation cross sections reported here are for transitions in helium ions from ground state to $\text{He}^+(n = 2)$ and $\text{He}^+(n = 3)$ in 20-100 keV collisions with neutral ground-state helium atoms.

II. ANALYSIS OF TRANSITIONS IN PROJECTILE

Energy-loss spectrometry involves detection and analysis of the incident beam projectiles. As the projectiles traverse the collision region, interacting with the target particles, they undergo a certain amount of angular scattering. However, in marked contrast to the behavior of electron projectiles, heavy particle scattering is confined almost entirely to extremely small angles about the forward direction, with scattering of the projectiles through angles appreciably different from zero being extremely rare.¹³ The pronounced concentration of the scattering in the forward direction was illustrated theoretically in 1933.¹⁴ These results have been verified experimentally¹⁵⁻¹⁷ by measuring cross sections as a function of angle about the forward direction.

Thus, the projectile beam may be described as being well-defined, both in and following the interaction region. The cross sections obtained from the UMR positive-ion energy-loss spectrometer, which collects the forward-scattered beam, are differential in energy loss. That is, these cross sections are essentially equivalent to the angular energy-loss doubly-differential cross sections integrated over all angles.¹⁸

The theory of positive-ion energy-loss spectrometry has been given elsewhere.¹⁹ The following discussion is an extension of that analysis to include transitions in the projectile.

For ion-atom impact collisions, the detected transitions for excitation of the projectile ions are superimposed on the ionization continuum of the atom. Capture-loss cycling, which also appears as a continuum, and energy-loss transitions due to double scattering may also be superimposed on the ionic transitions. However, these various responses are additive.¹⁹ The total background continuum can therefore be suppressed, exposing the ionic transitions for evaluation. The complications due to double scattering can be removed as described below.

The appropriate model for determining energy-loss cross sections for transitions in the projectile is shown in Fig. 1 for the transition σ_p . In this model, I_{10} represents the monoenergetic, unscattered incident beam current, and I_{1p} represents the monoenergetic beam, or partial beam, current generated by the σ_p - transition. In Fig. 1, σ_c represents the cross section for losses of the incident beam due to charge-changing interactions. Also,

$$\sigma_j' \equiv \sigma_j - \sigma_p \quad (1)$$

where σ_j represents the cross section for all other incident beam losses. The inelastic collision losses and the charge-changing losses for partial beam I_{1p} are not identical to those for the incident beam, since some of the projectiles in the former remain in an excited state throughout the remainder of the scattering region. These loss cross

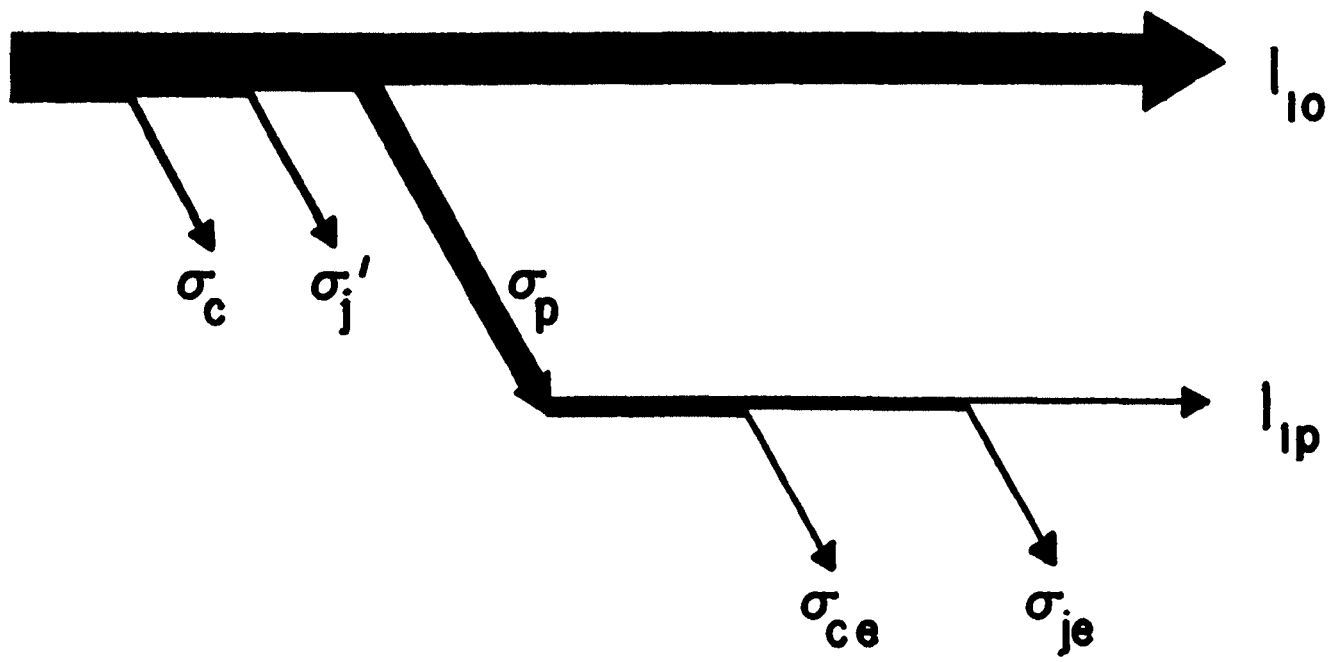


Fig. 1. Simplified partial beam model for projectile transitions.

sections for partial beam I_{lp} have an additional subscript to denote these differences (σ_{ce} and σ_{je}).

The differential equations describing the model in Fig. 1 are

$$dI_{10} = - I_{10}(\sigma_c + \sigma_j)n dx \quad (2)$$

and

$$dI_{lp} = I_{10}\sigma_p n dx - I_{lp}(\sigma_{ce} + \sigma_{je})n dx \quad (3)$$

where n is the number density of the target particles and dx is the differential scattering length measured along the collision path. With the boundary conditions $I_{lp} = 0$, $I_{10} = (I_{10})_i$ (where $(I_{10})_i$ is the incident current entering the scattering region) when $x = 0$, the solutions of Eqs.(2) and (3) for the beams emerging from the scattering region ($x = \ell$), are

$$(I_{10})_f = (I_{10})_i \exp[-(\sigma_c + \sigma_j)n\ell] \quad (4)$$

and

$$(I_{lp})_f = \frac{(I_{10})_f \sigma_p}{\lambda} [\exp(\lambda n \ell) - 1] \quad (5)$$

where

$$\lambda = (\sigma_c + \sigma_j) - (\sigma_{ce} + \sigma_{je}) . \quad (6)$$

If the quantity in Eq.(6) and the target particle density satisfy the "single collision" condition

$$\lambda n \ell \ll 1 \quad (7)$$

then the exponential in Eq.(5) can be approximated by

$$\exp(\lambda n \ell) \approx 1 + \lambda n \ell \quad (8)$$

which permits modification of Eq.(5) to the form

$$\sigma_p = \frac{1}{n \ell} \frac{(I_{1p})_f}{(I_{10})_f}, \quad \lambda n \ell \ll 1. \quad (9)$$

Since the approximation in Eq.(8) is mathematically equivalent to the assumption

$$\sigma_c + \sigma_j = \sigma_{ce} + \sigma_{je}, \quad (10)$$

Eq.(9) is identical to the results which are obtained for transitions in the target particles.¹⁹

To allow for possible differences between $\sigma_c + \sigma_j$ and $\sigma_{ce} + \sigma_{je}$ due to excitation of the projectiles, consider the approximation

$$\exp(\lambda n \ell) \approx 1 + \lambda n \ell + \frac{1}{2}(\lambda n \ell)^2. \quad (11)$$

Then, from Eq.(5),

$$(I_{1p})_f = (I_{10})_f \sigma_p n \ell (1 + \frac{1}{2} \lambda n \ell). \quad (12)$$

For the target pressure region where Eq.(12) is applicable, the σ_p cross section can be determined by least-squares fitting of experimental data for $(I_{1p})_f / (I_{10})_f$ versus reduced pressure, p_o , to an equation of the form^{19,20}

$$\frac{(I_{1p})_f}{(I_{10})_f} = a p_o + b p_o^2. \quad (13)$$

The reduced pressure is related to the target particle density:

$$n = N_L p_o \quad (14)$$

where N_L is Loschmidt's number

$$N_L = 3.54 \times 10^{13} \quad (15)$$

which is the number of molecules per cm^3 of ideal gas per unit reduced pressure. Also,

$$p_o = \left(\frac{273}{T}\right)p \quad (16)$$

where T is the absolute temperature in degrees Kelvin, and p is the target gas pressure in millitorr. Then, from Eq.(12), Eq.(13), and Eq.(14),

$$a = \sigma_p N_L^\ell \quad (17)$$

$$b = \frac{\sigma_p N_L^2 \ell^2 \lambda}{2} . \quad (18)$$

Since partial beams due to double scattering vary quadratically with the pressure,¹⁹ these complications are also separated from the linear variation with p_o . The σ_p ionic-transition cross section, in this approximation, can then be determined by using the linear least-squares constant in Eq.(17).

III. DESCRIPTION OF APPARATUS AND METHOD OF OPERATION

The University of Missouri - Rolla 250-kV acceleration-deceleration positive-ion energy-loss spectrometer was used to perform this study. This machine and the associated apparatus have been described in detail elsewhere.^{2,19} The following description is a summary of the basic features of the apparatus and the method of operation.

The He^+ ions were generated in a Colutron²¹ ion source by bombarding helium gas with electrons having a maximum energy of 40-eV (below lowest metastable state in helium ions). The ions extracted from this source had a kinetic energy distribution of approximately 0.1 eV. These ions were focused by an Einzel lens and were accelerated through a potential V (see Fig. 2). The energetic ions then impinged on the target gas which was contained in the center cell of a differentially pumped scattering chamber. The collision region, which had a length of 6.31 cm, was defined by two tantalum disks pierced with 0.051 cm-diam orifices. The pressure of the target gas was monitored with an MKS Baratron²² 77M-XRP differential pressure meter. A nulling signal from this meter was fed into a servo-amplifier feedback control system which automatically maintained the target gas pressure in the scattering chamber at any desired value.

The beam emerging from the scattering chamber was magnetically mass analyzed. The high-resolution energy analysis of the energy distribution of the emergent beam,

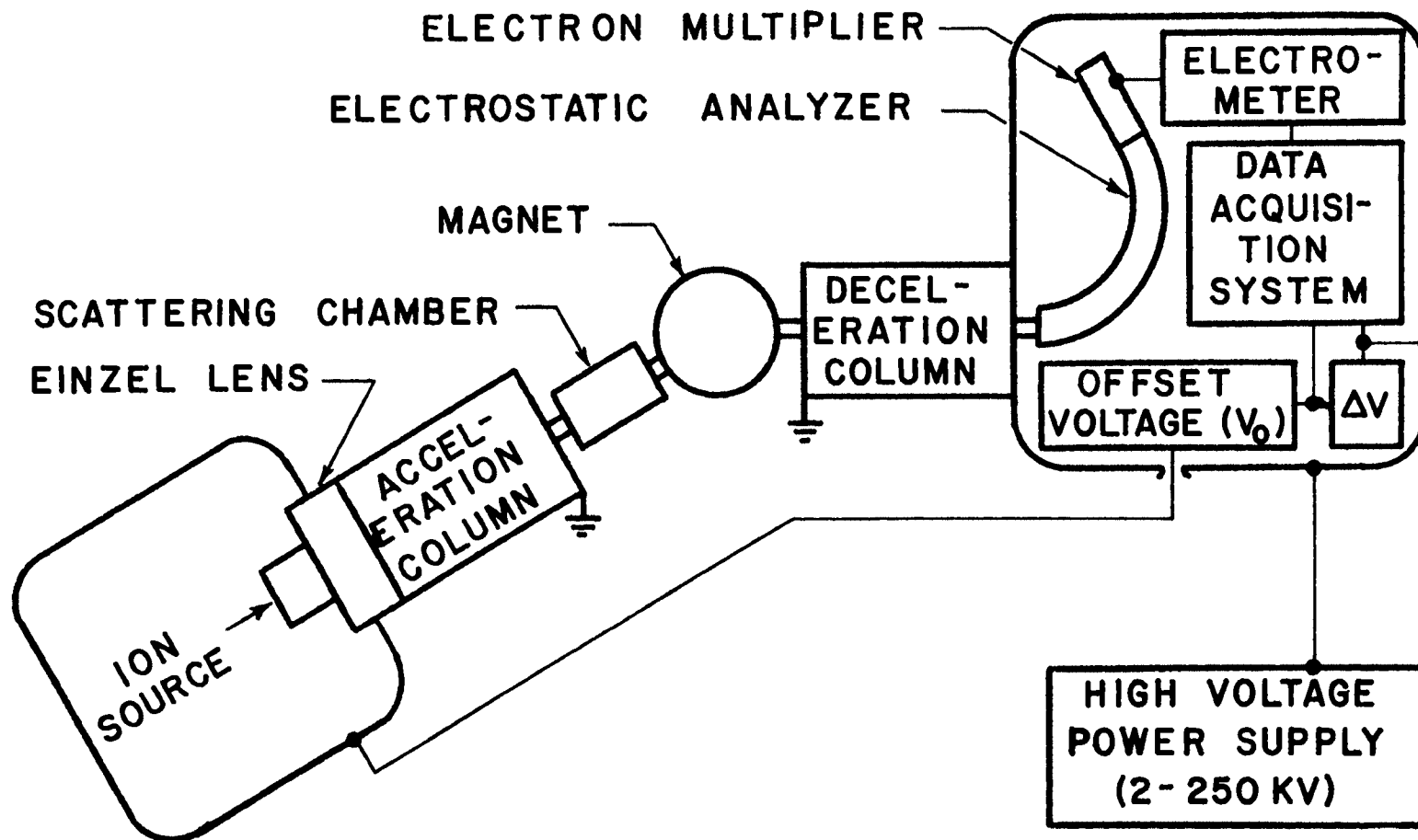


Fig. 2. Schematic diagram of UMR acceleration-deceleration positive-ion energy-loss spectrometer.

which is required in energy-loss spectrometry, was then accomplished by decelerating the ion beam to a low, well-defined energy, $eV_0 = 2 \text{ keV}$, before entering a 127° -electrostatic analyzer. With the analyzer plate voltage adjusted for maximum signal, the energy-loss spectrum was examined by slowly and continuously increasing the difference between the acceleration-deceleration potentials. This differential voltage, ΔV , was swept over the entire energy-loss range of interest, while maintaining the magnetic momentum analysis and the electrostatic energy analysis at fixed values.

Due to the kinetic energy distribution of the incident beam and due to the finite resolving power of the analyzer, a trace obtained without target gas in the scattering chamber, $\Phi(\xi)$, was a convolution of the energy spread in the ion beam and the dispersive effects of the apparatus. The magnitude of $\Phi(\xi)$, where ξ was the differential energy loss, was proportional to the beam current. Without altering any other experimental parameters, target gas was introduced into the scattering chamber, and ΔV was swept again. The trace then obtained, $R(\xi)$, the energy-loss spectrum, was a convolution of the incident beam energy distribution with the energy and angular effects of the apparatus and of the target gas. The procedure of modifying the accelerating potential by sweeping ΔV compensated for the corresponding energy lost in collisions with the target particles. This insured that all particles reaching the detector had traversed similar trajectories

between the scattering chamber and the detector, with energies lying within the same acceptance interval as any other particle reaching the detector. The magnitude of $R(\xi)$ was proportional to the emergent beam detected with n atoms/cm³ of target gas in the scattering chamber.

Typical traces of $\Phi(\xi)$ and $R(\xi)$ are shown in Figs. 3a and 3b for 50-keV He⁺ ions incident on helium gas (4 millitorr). The amplified output from the analyzer is shown as the ordinate and the differential energy loss, ξ , as the abscissa. The peak at the left of each trace is due to transmitted and elastically scattered projectiles. The first two essentially resolved peaks in the energy-loss spectrum of Fig. 3b correspond to discrete inelastic transitions in the target helium atoms. The discrete peaks superimposed on the ionization continuum of the target particles are excitation transitions in the He⁺ projectiles. The mathematical relationship between these two traces, R and Φ , and inelastic transitions has been described in detail elsewhere.¹⁸ The result of that analysis is briefly outlined below.

Since the two functions $R(\xi)$ and $\Phi(\xi)$ were plotted under the same experimental conditions with the introduction of target gas into the scattering chamber being the only distinguishing factor, the following relationship holds:

$$R(\xi) = n\ell \int \Phi(\xi - \xi') \frac{d\bar{\sigma}(\xi')}{d\xi} d\xi' \quad (19)$$

where

$$\frac{d\bar{\sigma}}{d\xi} \equiv \int_{\Delta\Omega} \frac{d^2\sigma(\theta, \xi)}{d\Omega d\xi} d\Omega \quad . \quad (20)$$

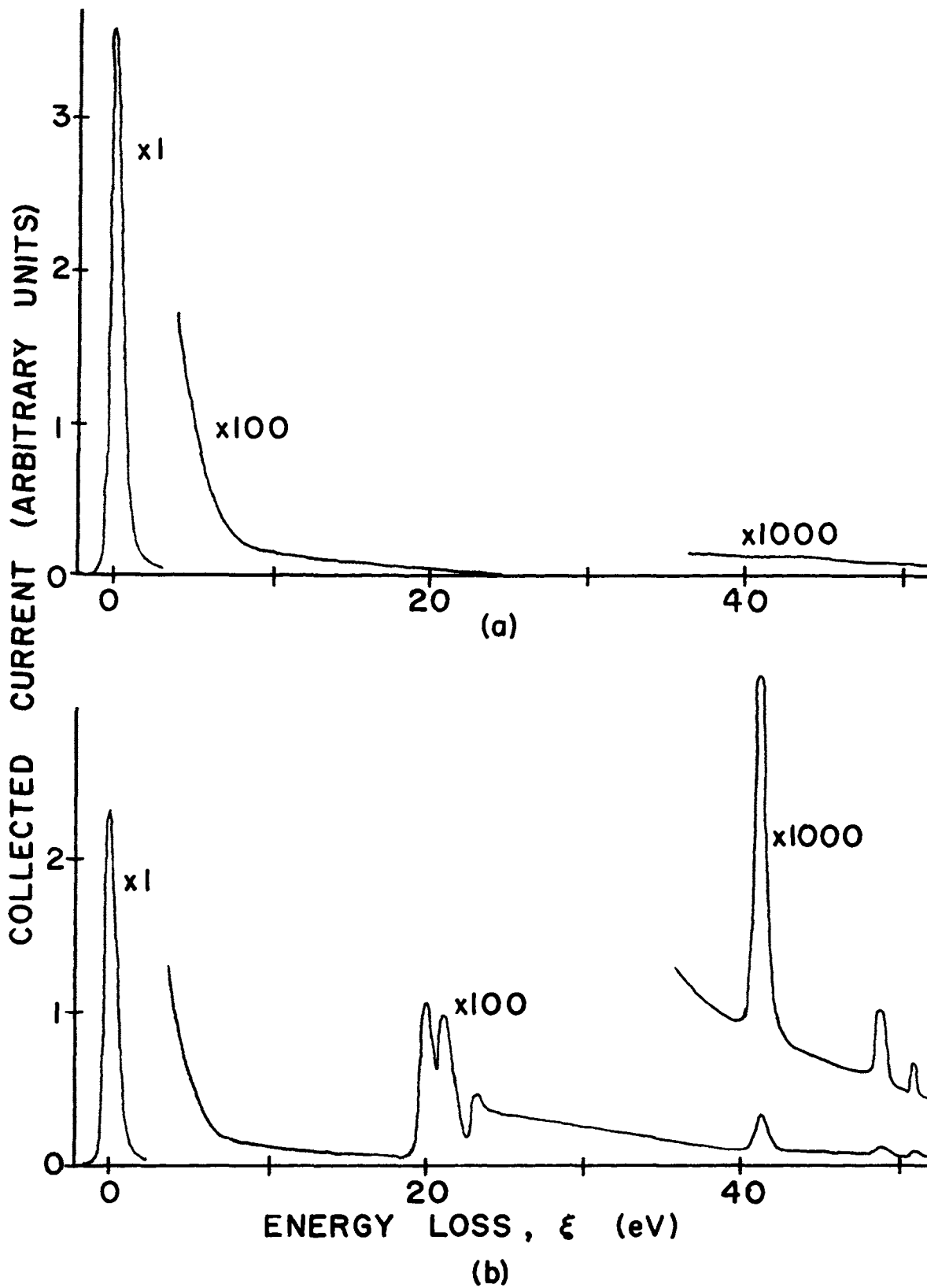


Fig. 3. Energy-loss traces (a) without target gas, and (b) with target gas.

$d^2\sigma/d\Omega d\xi$ is the doubly-differential cross section per unit angle per unit energy loss for scattering into the solid angle $d\Omega$ and energy-loss interval $d\xi$. ξ is a (positive) energy loss as measured from the most probable energy of the decelerated, elastically-scattered ion beam. θ and $\Delta\Omega$ are the laboratory scattering angle and the instrumental acceptance solid angle, respectively. Due to the predominant peaking in the forward direction in positive-ion energy-loss spectrometry,^{13,18} essentially all of the scattered, singly-charged projectiles are detected. Then, the experimentally determined cross section is equivalent to the energy-loss differential cross section to the extent that

$$\frac{d\bar{\sigma}(\xi)}{d\xi} = \int_{4\pi} \frac{d^2\sigma(\theta, \xi)}{d\Omega d\xi} d\Omega = \frac{d\sigma(\xi)}{d\xi} \quad (21)$$

To determine absolute cross sections, it is necessary to assume that the elastic and inelastic contributions to $R(\xi)$ are separable. Then, if the transition responsible for a peak in the energy-loss spectrum can be identified, and if $R(\xi)$ with the background suppressed drops essentially to zero on each side of the peak, integration of R over the peak yields the total cross section for that transition. For example, in the pressure range over which Eq.(9) is applicable, the cross section determined from a peak in the energy-loss spectrum is

$$\sigma_p = \frac{\int_{\Delta\xi_p} R(\xi) d\xi}{n\ell \int_{\Delta\xi_0} R(\xi) d\xi} = \frac{1}{n\ell} \frac{(I_{1p})_f}{(I_{10})_f} \quad (22)$$

where $\Delta\xi_p$ is the interval corresponding to the transition peak, and $\Delta\xi_o$ is the interval corresponding to the elastic and transmitted region of $R(\xi)$. The calculated cross sections are "absolute" in the sense that they are not normalized to other data or theory.

IV. DATA

The data for this study were taken with helium-ion impact energies ranging between 20-100 keV, in 10-keV intervals. Most of the data were taken with overall apparatus resolution between 0.6-0.8 eV FWHM. The target thicknesses ranged between 3-50 millitorr-cm. The two energy-loss peaks of primary interest were situated at 40.8 ± 0.1 and 48.4 ± 0.2 which correspond to excitation of the ground-state helium-ion projectiles to the second and third principal quantum levels. An enlarged view of the relative energy locations of the quantum states within these two principal levels is shown in Fig. 4. As the energy separations between the various states within a quantum level of He^+ are much too small to be resolved, transitions to the various states within a level contribute to a single peak observed at the energy loss corresponding to the excitation energy of this level above the ground state of the helium ion.

To calculate the cross sections for these two transitions at a given energy, it was necessary to suppress the background continuum, which results primarily from ionization of target He atoms. The background for each transition was obtained by drawing in a baseline which smoothly joined the background on each side of the peak. This background was then subtracted, exposing the peak for cross section evaluation. To subtract off the continuum in this manner, it must

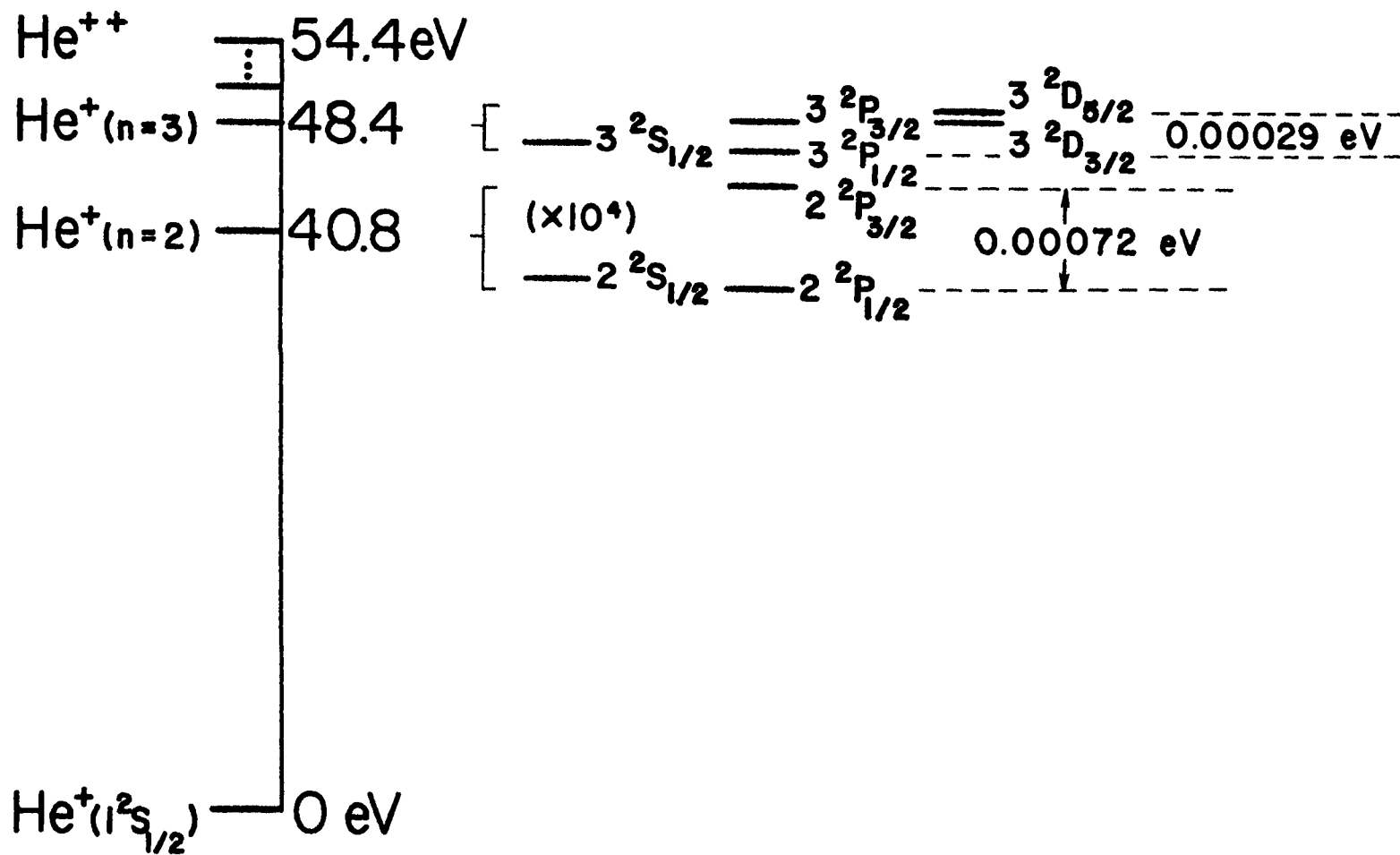


Fig. 4. Energy level diagram of He⁺. (Data taken from C. E. Moore, Atomic Energy Levels, Nat. Bur. of Standards Circular 467, June 15, 1949.)

be assumed that the background in the absence of the ionic transitions is slowly varying, containing no structure. The ionization continuum of the helium target gas and the capture-loss continuum satisfy this criterion. The possibility of structural transitions superimposed on the continuum at the location of the ionic transitions can arise primarily from two possible sources: (i) double scattering, and (ii) autoionizing transitions. The double scattering complication is removed by the quadratical least-squares fitting of the data as discussed above. The lowest autoionizing energy-loss transition occurs for $\text{He}(1s^2)^1S \rightarrow \text{He}(2s^2)^1S$ at 57.9 eV.²³ This is sufficiently remote from the energy loss corresponding to the two ionic transitions measured in this experiment that disturbances due to autoionizing transitions are nonexistent. But, if a target particle should be excited by a projectile and then, while still excited, undergo another excitation into an autoionizing level by a collision with a second projectile, the energy loss of this second collision could be superimposed on the detected ionic transitions. However, the scattering density for interactions between projectiles and other collision products is less than 10^{-8} of those for interaction with the target particles themselves.¹⁹ The disturbing influence from the appearance potentials of autoionizing levels therefore can be neglected.

Cross sections for excitation of helium ions to

$\text{He}^+(n = 2)$ and $\text{He}^+(n = 3)$ in collisions with helium atoms have been calculated by the method outlined above. These cross sections are shown in Figs. 5 and 6 as a function of impact energy. (The smooth curve sketched through the values plotted in Fig. 6 has been reproduced in Fig. 5 to permit comparison of magnitudes.) The error bars shown are vectorial additions (rms values) of the random standard deviations obtained from the least-squares analyses and of an estimated maximum systematic error of 10%, which was largely due to estimated uncertainty in the pressure measurements. These cross-sections plotted as a function of impact energy are still rapidly increasing at 100 keV. Within the limits prescribed by the error bars, it appears that the peaks for these curves are situated well above 100 keV. The measurement of cross sections of this order of magnitude ($\sim 10^{-20} \text{ cm}^2$) extends the technique of positive-ion energy-loss spectrometry until it encompasses most of the range covered by experiments observing secondary emission.

In some of the energy-loss data, transitions of the ground-state helium-ion projectiles to the fourth and fifth principal quantum levels were also resolved. The statistics for these transitions were not sufficient to report calculated cross sections; however, the n^{-3} law²⁴ did not appear to be obeyed for excitation to these lower levels in the helium ion.

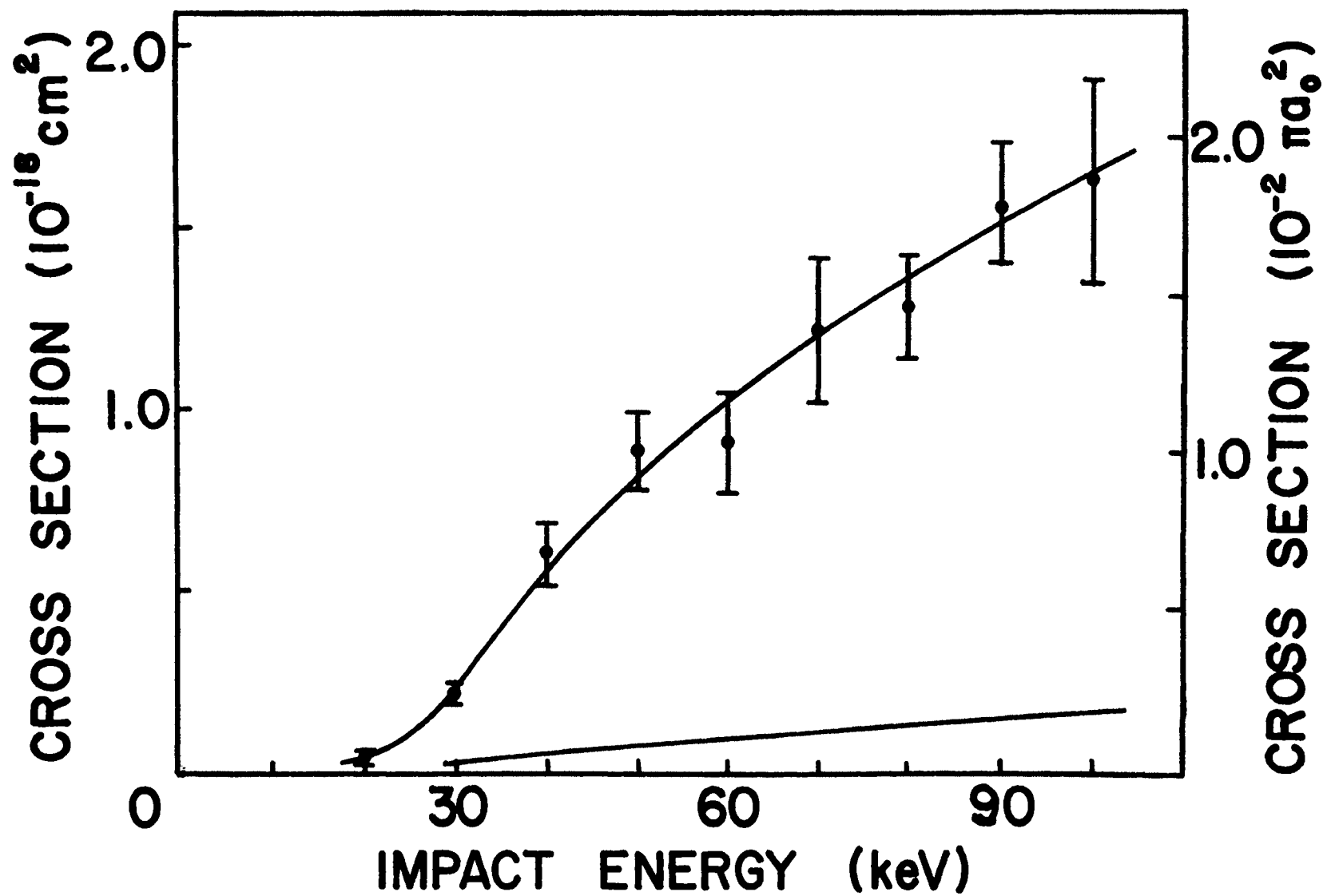


Fig. 5. Absolute $\text{He}^+(1^2s_{1/2}) \rightarrow \text{He}^+(n=2)$ ionic transition cross section as a function of impact energy (with He).

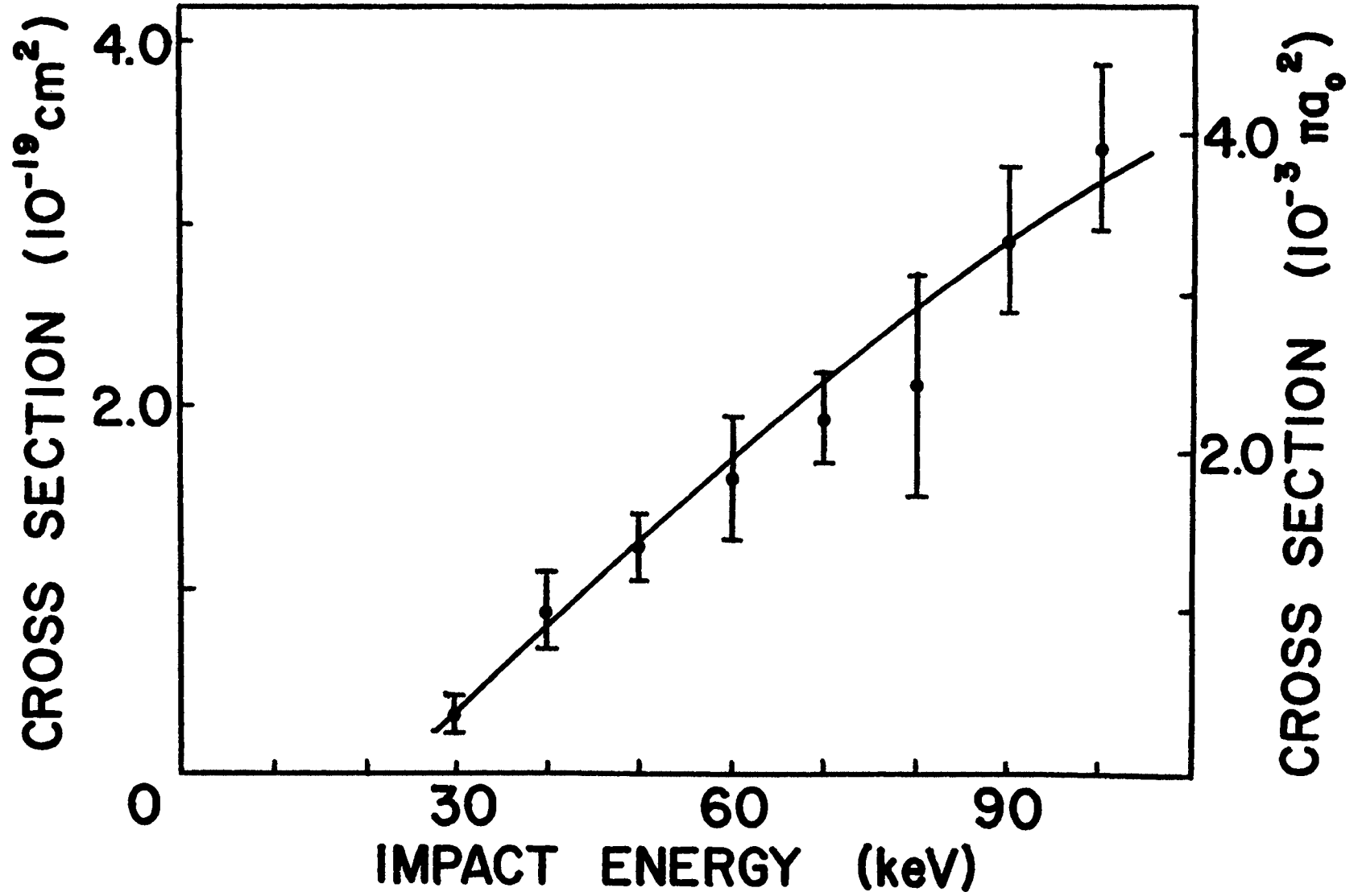


Fig. 6. Absolute $\text{He}^+(1^2s_{1/2}) \rightarrow \text{He}^+(n=3)$ ionic transition cross section as a function of impact energy (with He).

V. DISCUSSION

To the author's knowledge, there are no existing theoretical calculations or experimental determinations with which to directly compare the results of this study. Complete analytical calculations for making a comparison are nonexistent because of the impossibility of obtaining exact solutions for atomic collision cross sections. For any atom more complex than hydrogen, the wave functions are only approximately known, and are frequently non-orthogonal. Further, the complexity of the equations is such that approximate methods must be employed even if the exact wavefunctions were known. Also, the commonly applied approximations are not really valid for He^+ projectiles in the impact energy range covered in this study.

A few experiments have been performed for evaluating the characteristics of quantum excitations in helium ions. In particular, a crossed-beam method has been used to measure the cross section of $\text{He}^+(1s) \rightarrow \text{He}^+(2s)$ by electron impact for energies ranging from threshold to 750 eV.²⁵ The results of this experiment showed that, at the higher energies, the energy dependence of the cross section is in close agreement with that calculated by means of the plane-wave Born approximation. Most other studies concerning He^+ have involved simultaneous excitation-ionization of helium atoms by electron or proton impact.²⁶

As mentioned earlier, ionic excitation transitions have

been observed by Boudon et al.⁵ for He^+ impacting with He. These experiments were performed with a maximum impact energy of 3 keV. The published data showing the ionic transition was for the scattered beam collected at 3° from the forward direction. Boudon et al., claimed that a collision in which the ion becomes excited while the atom remains unexcited seems very improbable. Looking at Figs. 5 and 6, ionic excitation transitions for the He^+ -He system are quite probable for impact energies above 20 keV. However, if the curves in Figs. 5 and 6 were extrapolated backward into the energy region covered by the experiments of Boudon et al., the cross-sections, even for total scattered current, are indeed very small, probably less than 10^{-20} cm^2 .

Technically, the cross sections determined in this study probably could be measured using crossed-beam techniques. However, absolute measurements using crossed beams would be difficult.

Radiative transitions following He^+ -He collisions from levels of $\text{He}^+(n = 3)$ to levels of $\text{He}^+(n = 2)$ should be measurable with ultra-violet spectroscopy. Although the correlation would be indirect, it would be interesting to compare such optical emission measurements with these measurements obtained by energy-loss spectrometry.

It is hoped that the experimentally determined cross sections obtained in this study will provide new insight into currently observed physical phenomena and will contribute to

the advancement of the theoretical investigations of atomic structures as embodied in collision cross sections.

VI. APPENDICES

A. Theory of Positive-Ion Energy-Loss Spectrometry

Energy-loss spectrometry involves analysis with fast projectiles having energies orders of magnitude greater than normal thermal energies. With these fast projectiles, space charge difficulties are essentially negligible and are further minimized as the projectile energy is increased, making it possible to obtain well-defined beams of ions. However, in the following discussion, the velocities are assumed to be sufficiently low that relativistic and nuclear effects may be ignored. For relativistic effects, this assumption is valid up to energies of several tens of MeV for heavy particle impact. Nuclear effects, however, become important when the quantum-mechanical wavelength of the projectile is of the order of 10^{-12} cm,²⁷ which corresponds to an energy of approximately 1 MeV for He⁺ ions.

In the following discussion, the gaseous target is assumed to be comprised of a single atomic species, with the particles considered to be at rest. The incident beam is assumed to be parallel, monoenergetic, homogeneous, and comprised of a single ionic species.

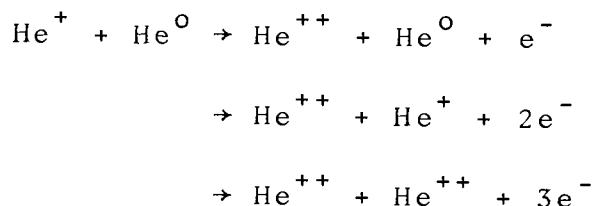
As the projectiles impinge on the target particles, various processes can occur. In any given collision between a projectile and a target particle, the probability of the occurrence of a particular type of interaction under given conditions depends on the nature of the collision partners,

on their mutual velocity of approach, and the impact parameter of the collision.²⁸ This probability is conventionally expressed in terms of a microscopic cross section, usually denoted by σ , having units of $\text{cm}^2/\text{target-particle}$, or units of $\pi a_0^2 = 0.88 \times 10^{-16} \text{cm}^2$, where $a_0 = 0.53 \times 10^{-8} \text{cm}$ is the radius of the first Bohr orbit of the hydrogen atom. The total microscopic cross section for a particular interaction represents the total "area" presented by each of the target particles for projectile scattering into the total solid angle, 4π steradians. Since this is the quantity effectively measured in positive-ion energy-loss spectrometry, the following discussion is centered entirely on these total microscopic cross sections, which are referred to as simply "cross sections" for convenience.

As the projectile beam traverses the scattering region, its composition changes due to various charge-changing and inelastic collisions. Of the various charge-changing collisions which can occur, two are of primary importance:

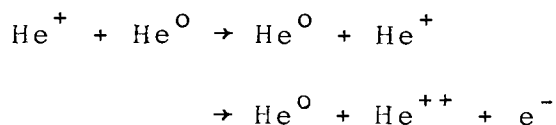
(i) stripping (ejection of an electron from a projectile into the continuum) of the beam projectiles, leaving them in a doubly-charged state, and (ii) neutralization of the beam projectiles by electron-capture from the target atoms.

The stripping of projectiles is usually described by a stripping, or detachment, cross section, usually denoted by σ_ℓ , which is the total probability that a fast incident ion loses an electron. For the $\text{He}^+ - \text{He}$ collision system, the most important reactions which contribute to stripping are



with the predominant contribution coming from the second interaction listed.²⁹ For fast He^+ ions, $\sigma_\ell \ll \sigma_i$,³⁰ where σ_i is the ionization cross section of the target particles.

The neutralization of the projectile can leave the projectile in either the ground state or in an excited state, and is usually described by a capture cross section. The most important reactions of this type for the He^+ -He collision system are



with the predominant contribution coming from the first interaction listed,²⁹ and of these interactions, those which leave the neutralized projectile in the ground state are referred to as symmetrical resonance charge transfer. In an ion-atom collision, the cross section for resonance charge transfer is much larger than the cross section for transitions between states with different angular momenta by virtue of the different symmetry of these states.³¹ This was experimentally verified when beams of fast helium atoms produced by charge exchange were found to contain no appreciable admixture of metastable atoms, as indicated by the equality $\sigma_i = \sigma_\ell$ for

the interaction of the fast neutralized helium projectiles with helium gas.³²

The projectiles which have undergone the various charge-changing interactions and the various energy-loss processes constitute an array of smaller beams within the incident beam, or partial beams. Those having different energy losses can, ideally, be viewed individually by energy analyzing the beam emerging from the scattering region. A diagrammatic representation of the noninteracted incident monoenergetic beam, the inelastic energy-loss partial beams, and the charge-changed partial beams are shown in Fig. A1.

Expressing a partial beam in terms of an electrical current, which is the physical quantity actually measured in energy-loss spectrometry,

$$I_{jk} = n_s e v A \quad (A1)$$

where n_s is the particle density of the ions in the partial beam, e is the fundamental electronic charge, v is the velocity of these monoenergetic projectiles, and A is the cross-sectional area of the beam. The first subscript on the current, j , indicates the charge-state of the projectiles, while the second subscript, k , indicates the energy-difference of these projectiles relative to those of the incident beam. An additional subscript of i or f indicates respectively the incident beam or the detectable beam emerging from the scattering region. Currents with only one subscript compositely symbolize all partial beam currents in the charge-state

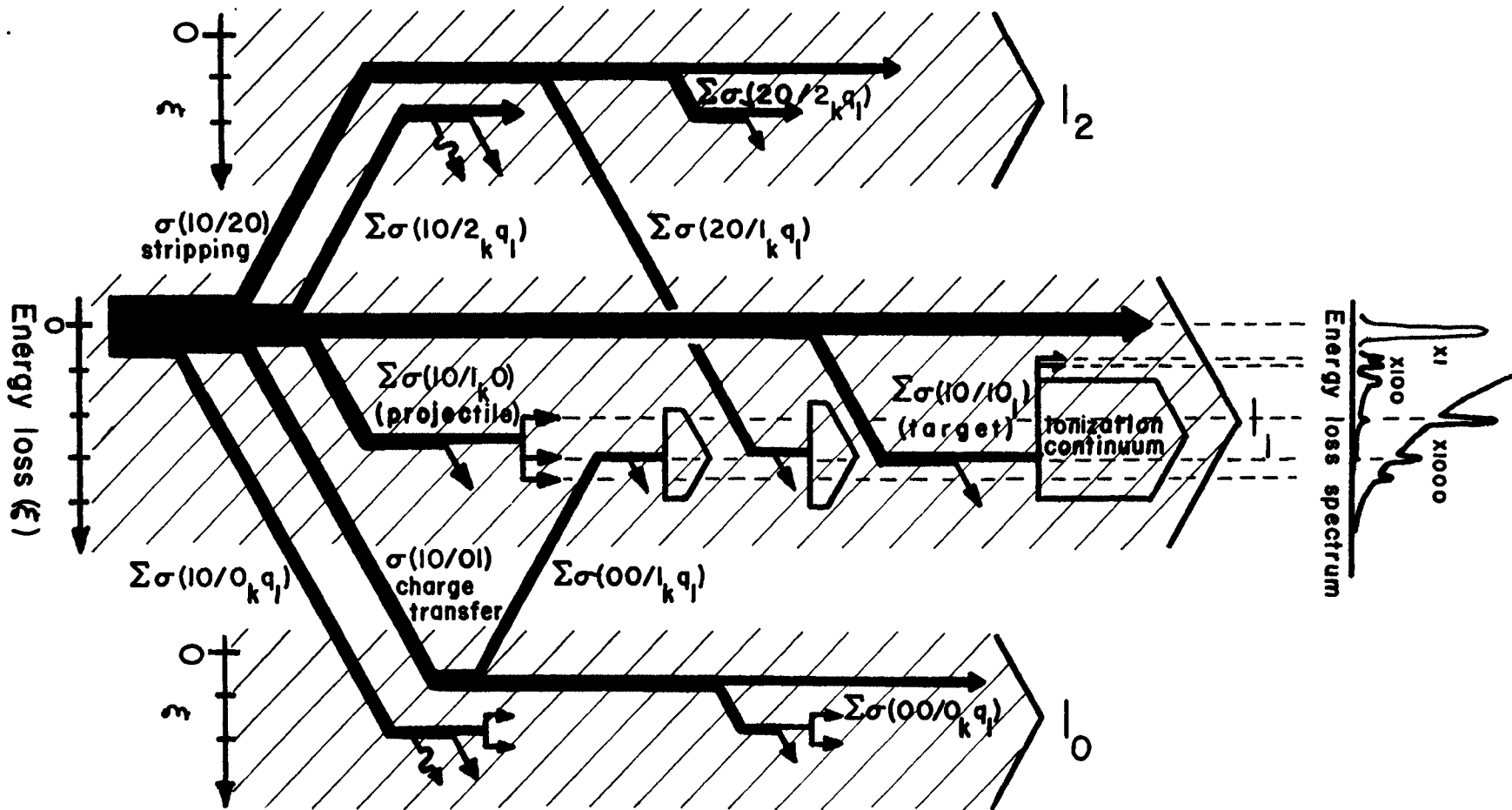


Fig. A1. Representative partial beam generation and loss contributions in scattering region; energy distribution of composite beams I_0 and I_2 not observed.

represented by that single subscript, irrespective of the energy difference of the various partial beams in that charge state.

The cross section describing a particular interaction in Fig. A1 is to be interpreted typically as follows:

$$\sigma(a_i b_j / c_k d_\ell)$$

implies an interaction where the projectile in charge-state a and energy-state i collides with a target particle in charge state b and energy state j , leaving the post-collision projectile in charge-state c , etc. The absence of a subscript indicates a ground-state configuration for that particular collision partner.

The two radiation vectors shown in Fig. A1 do not actually represent a loss, but indicate that projectiles in those partial beams can change excitation states by radiative transitions. Projectiles in some of the other partial beams can undergo similar transitions, but radiative transitions have negligible effect on the energy-loss data and are subsequently ignored.

From each of the partial beams, there are losses due to the occurrence of additional inelastic and charge-transfer collision processes before the partial beam particles emerge from the scattering region. In most cases, these losses do not affect the final observed results, and are indicated in Fig. A1 by dangling loss vectors. Those loss components which do take an active role in the final analysis are elaborated upon in more detail where warranted in the following

discussion.

Of particular interest are the $\sigma(10/1_k 0)$ and $\sigma(10/10_\ell)$ interactions between the incident beam and the target particles (see Fig. A1). The former represents excitation transitions in the projectile ions, and the latter represents inelastic transitions in the target particles.

All of the singly-charged partial beams in the scattering region are compositely labeled I_1 in Fig. A1. Similarly, the neutralized partial beams and the doubly-charged partial beams are compositely represented by I_0 and I_2 , respectively. Theoretically, charge-changing collisions can occur between any partial beam in one composite beam and a partial beam in another composite beam. However, it will now be shown that interactions between partial beams (or beam-beam interactions) are negligible in comparison to those occurring between a partial beam and the target particles. For discussion purposes, the beam-beam interaction argument is focused on interactions between a partial beam, I_{1s} , and the unscattered incident beam, I_{10} . The results, however, are applicable to any beam-beam interaction in the scattering region.

Equation (A1) can be used to determine the current of the unscattered beam as seen by another partial beam having a different velocity (energy) if one beam is expressed as a particle density, and v in Eq.(A1) represents the relative velocity between these two beams. For the unscattered incident beam,

$$eV = \frac{1}{2}mv^2 \quad (A2)$$

where V is the accelerating potential, and m is the mass of the projectiles. Combining Eqs.(A1) and (A2), the projectile beam current expressed as a particle density becomes

$$n_s = \frac{I_{10}}{Ae} \sqrt{\frac{m}{2eV}} \quad (A3)$$

Then, for the usual form of loss (or gain) term,

$$\begin{aligned} dI_{10} &= I_{10} \sigma n_s dx \\ &= \frac{I_{10}}{Ae} \sqrt{\frac{m}{2eV}} e(v - v_s) A \sigma \frac{I_{1s}}{Ae} \sqrt{\frac{m}{2eV_s}} dx \\ &= I_{10} \sigma \left[\frac{I_{1s} m (v - v_s)}{2Ae^2 \sqrt{VV_s}} \right] dx \end{aligned} \quad (A4)$$

where v_s differs only slightly from the velocity of the unscattered beam, the difference corresponding to the energy loss, ΔE , of the interaction generating the scattered beam:

$$v_s = \sqrt{\frac{2eV_s}{m}} = \sqrt{\frac{2(eV - \Delta E)}{m}} \quad (A5)$$

Now

$$\sqrt{VV_s} \approx V \quad (A6)$$

and

$$\begin{aligned} v - v_s &= \sqrt{\frac{2eV}{m}} - \sqrt{\frac{2(eV - \Delta E)}{m}} \\ &= \sqrt{\frac{2eV}{m}} \left(1 - \sqrt{1 - \frac{\Delta E}{eV}} \right) \end{aligned} \quad (A7)$$

Since $\Delta E \ll eV$, the radical in Eq.(A7) can be very closely

approximated by

$$\sqrt{1 - \frac{\Delta E}{eV}} \approx 1 - \frac{1}{2} \left(\frac{\Delta E}{eV} \right) .$$

Then,

$$v - v_s \approx \frac{\Delta E}{\sqrt{2meV}} . \quad (A8)$$

Substituting Eqs.(A6) and (A8) into Eq.(A4),

$$I_{10} \sigma n_s dx \approx I_{10} \sigma n_{\text{eff}} dx \quad (A9)$$

where

$$n_{\text{eff}} = \frac{I_{1s} \Delta E}{2Ae^2 V} \sqrt{\frac{m}{2eV}} . \quad (A10)$$

The relative importance of contributions due to beam-beam interactions can be determined by evaluating the ratio of n_{eff} to n , the particle density of the target. Now I_{1s} was presumably generated by interactions between the incident beam and the target gas, indicating that I_{1s} and the target particle density are interrelated. This relationship can be approximated by

$$\frac{I_{1s}}{n} \approx \sigma \ell (I_{10})_i \quad (A11)$$

where σ is the cross section describing the production of I_{1s} , and ℓ is the length of the entire distance over which the projectiles in both beams have intermingled trajectories. Using Eq.(A11) and typical values consistent with those of

the UMR positive-ion energy-loss spectrometer, for over-extreme (worst case) conditions,

$$\frac{n_{\text{eff}}}{n} \sim 10^{-8} . \quad (\text{A12})$$

This indicates that cross sections for beam-beam interactions can be many orders of magnitude larger than cross sections for beam-target interactions, and the contribution still remain negligible. These results are obviously applicable to interactions between any two partial beams.

Besides losses, there may be additional generation contributions to the various partial beams in Fig. A1. The coincidence of energy loss for a partial beam generated by a single discrete transition with a partial beam generated by the resultant of multiple, discrete energy-loss transitions would be largely accidental. However, a commonly occurring situation involves the superposition of a transition into a discrete state and transitions into a continuum at a given energy loss. Another source of partial beam generation arises from stripping collisions between fast neutralized projectiles and target particles (see transitions $\Sigma\sigma(00/1_k q_\ell)$ in Fig. A1). These contributions will also appear in the form of a continuum. If the total contributions to the continuum result in a background which is continuous and slowly varying in the vicinity of a superimposed discrete transition, it is shown below that the cross section for the discrete transition can be determined by suppressing this background.

Obviously the complexity of the coupling between the various partial beams via interaction with the target gas proposes an intractable analytical problem. The magnitude of most of these coupling effects are much smaller than the primary generation and loss contributions. Also, most experiments are performed under conditions which approximate single-collision conditions. Therefore, considerable simplification can be made through appropriate approximations, which still yield sufficiently accurate first order corrections. The approximations will now be applied to each facet of the essentials required for interpreting the data for experimental collision cross sections from positive-ion energy-loss spectrometry.

1. Charge-Changing Interactions. With magnetic deflection apparatus following the scattering region which separates composite beam I_1 from composite beams I_0 and I_2 , the essential charge-changing cross sections can be experimentally determined. Although these cross sections do not enter explicitly into the final calculations of the discrete energy-loss transitions, the results are useful in describing the transitions.

The simplified composite beam model for sufficiently accurate first order determinations of the essential charge-changing cross sections is shown in Fig. A2. The mutual gain-loss contributions through charge-transfer beam-beam interactions have been ignored (see discussion above). The

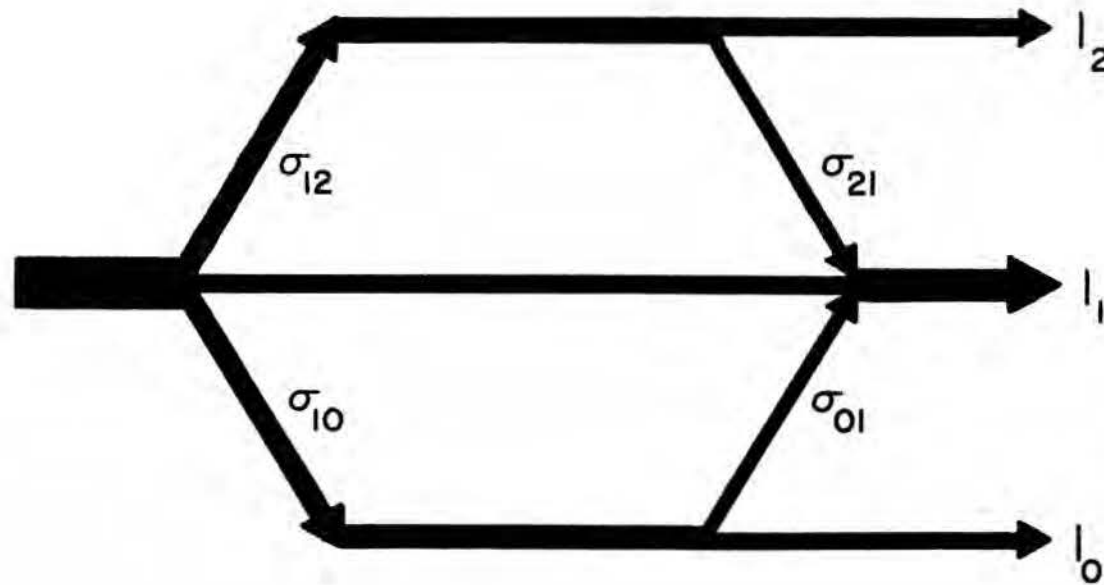


Fig. A2. Simplified composite beam model for charge-changing interactions.

specified cross sections represent the transitions between the composite beams. The differential equations describing this model are:

$$dI_0 = I_1 \sigma_{10} n dx - I_0 \sigma_{01} n dx \quad (A13)$$

$$dI_2 = I_1 \sigma_{12} n dx - I_2 \sigma_{21} n dx \quad (A14)$$

$$dI_1 = -(dI_0 + dI_2) . \quad (A15)$$

Then, with the boundary conditions $I_1 = (I_{10})_i$, $I_0 = I_2 = 0$ when $x = 0$, Eqs.(A13), (A14), and (A15) yield the solution for the detectable, singly-charged beam emerging from the scattering region ($x = \ell$), $(I_1)_f$:

$$(I_1)_f = (I_{10})_i \left[C_1 + C_2 \exp[-(\gamma + 2\chi)\frac{n\ell}{2}] + C_3 \exp[-(\gamma - 2\chi)\frac{n\ell}{2}] \right] \quad (A16)$$

where

$$C_1 = \frac{\sigma_{21}\sigma_{01}}{\sigma_{12}\sigma_{01} + \sigma_{21}\sigma_{10} + \sigma_{21}\sigma_{01}}$$

$$C_2 = \frac{(\sigma_{12} + \sigma_{10} + 2\chi)^2 - (\sigma_{21} - \sigma_{01})^2}{4\chi(\gamma + 2\chi)}$$

$$C_3 = \frac{(\sigma_{21} - \sigma_{01})^2 - (\sigma_{12} + \sigma_{10} - 2\chi)^2}{4\chi(\gamma - 2\chi)}$$

$$4\chi^2 = (\gamma - 2\sigma_{01})^2 - 4\sigma_{10}(\sigma_{21} - \sigma_{01})$$

and

$$\gamma = \sigma_{12} + \sigma_{21} + \sigma_{10} + \sigma_{01}$$

which obviously is not in a convenient form for experimental application. However, in evaluating cross sections, the incident monoenergetic beam is the primary normalizing constituent. Regeneration through the $\sigma_{12} - \sigma_{21}$ and the $\sigma_{10} - \sigma_{01}$ sequences cannot be realized without energy loss, indicating that although the σ_{21} and σ_{01} interactions are sources for I_1 , they are not generation sources for the incident monoenergetic beam. Thus, the total charge-changing cross section, σ_c , where

$$\sigma_c = \sigma_{12} + \sigma_{10} \quad (\text{A17})$$

is the actual quantity affecting inelastic cross section calculations. By letting

$$\alpha = \frac{(I_1)_f}{(I_{10})_i} \quad (\text{A18})$$

and taking the derivative with respect to the reduced pressure; then, in the limit as the reduced pressure goes to zero,

$$\lim_{p_o \rightarrow 0} \frac{d\alpha}{dp_o} = -\lambda N_L (\sigma_{12} + \sigma_{10})$$

or

$$\sigma_c = -\frac{1}{\lambda N_L} \left\{ \lim_{p_o \rightarrow 0} \frac{d\alpha}{dp_o} \right\} . \quad (\text{A19})$$

This result indicates that the total charge-changing cross section for the incident beam can be evaluated from the

asymptotic value of the slope of α versus reduced pressure as the target gas pressure is extrapolated to zero.

If the target gas pressure is sufficiently low that single-collision conditions are approximately satisfied, then

$$\alpha \approx e^{-\sigma_c n \ell} . \quad (\text{A20})$$

Fitting experimental data for α versus reduced pressure to an equation of the form

$$\alpha = e^{-a_c p_0} \quad (\text{A21})$$

by the method of least-squares yields,

$$a_c = - \frac{\sum p_{on} \ln \alpha_n}{\sum p_{on}^2} \quad (\text{A22})$$

where, from Eq. (A20),

$$a_c = \sigma_c N_L \ell . \quad (\text{A23})$$

Then, in this approximation,

$$\sigma_c = \frac{a_c}{N_L \ell} (1 \pm \epsilon_c) . \quad (\text{A24})$$

In this equation, ϵ_c is the relative standard deviation

$$\epsilon_c = \sqrt{\frac{\sum (\delta \ln \alpha_n)^2}{a_c^2 (k-1) \sum p_{on}^2}} \quad (\text{A25})$$

where

$$\sum (\delta \ln \alpha_n)^2 = \sum (\ln \alpha_n)^2 + a_c^2 \sum p_{on}^2 + 2 a_c \sum p_{on} \ln \alpha_n \quad (\text{A26})$$

and k is the number of data samples.

2. Transitions in Target. For inelastic transitions in the target particles, the simplified model for sufficiently accurate first order corrections is shown in Fig. A3 for the transition $\sigma_a \equiv \sigma(10/10_a)$. Here, σ_j' is equal to σ_j less the cross section for the observed transition in the target:

$$\sigma_j' \equiv \sigma_j - \sigma_a . \quad (\text{A27})$$

The beam-beam interactions have been ignored in Fig. A3. Also, by temporarily limiting the discussion to inelastic transitions with energy losses lower than the ionization potential, the contributions due to $\Sigma\sigma(00/1_k q_\ell)$ interactions can be neglected.

The differential equations describing the model in Fig. A3 are:

$$dI_{10} = -I_{10}(\sigma_c + \sigma_j)n dx \quad (\text{A28})$$

$$dI_{1a} = I_{10}\sigma_a n dx - I_{1a}(\sigma_c + \sigma_j)n dx . \quad (\text{A29})$$

With the boundary conditions $I_{10} = (I_{10})_i$ and $I_{1a} = 0$ when $x = 0$, the detectable current ($x = \ell$) solutions for these equations are:

$$(I_{10})_f = (I_{10})_i \exp[-(\sigma_c + \sigma_j)n\ell] \quad (\text{A30})$$

$$(I_{1a})_f = (I_{10})_i \sigma_a n \ell \exp[-(\sigma_c + \sigma_j)n\ell] . \quad (\text{A31})$$

In this derivation, σ_c and σ_j are considered to have the same

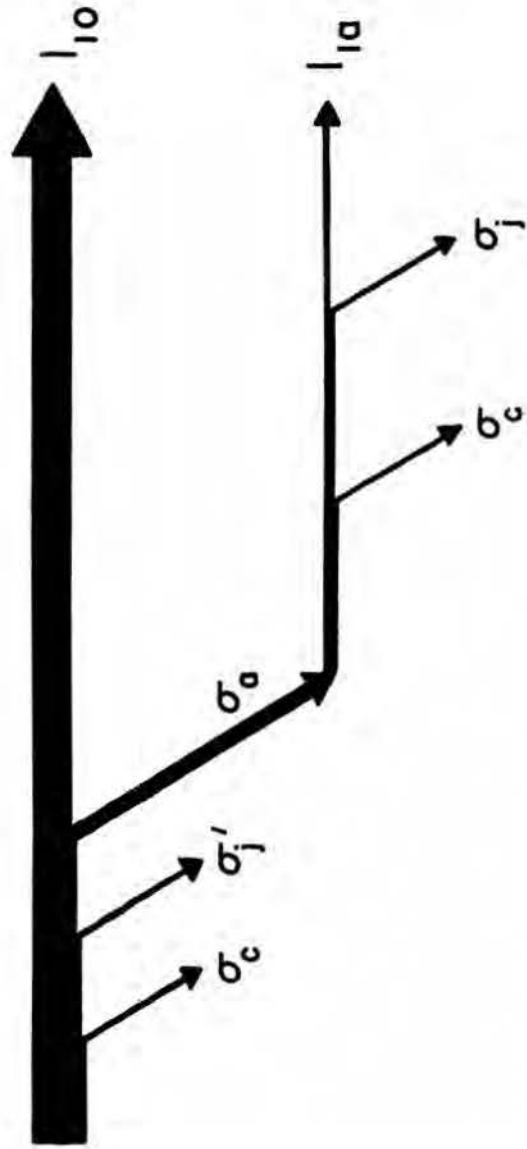


Fig. A3. Simplified partial beam model for target transitions.

values for both I_{10} and I_{1a} which justifiably ignores the negligible differences due to the slight loss of energy for the σ_a -transition. Combining Eqs.(A30) and (A31),

$$\sigma_a = \frac{1}{n\ell} \frac{(I_{1a})_f}{(I_{10})_f} . \quad (\text{A32})$$

The relative detectable scattered current, α_a ,

$$\alpha_a = \frac{(I_{1a})_f}{(I_{10})_i} \quad (\text{A33})$$

as a function of reduced pressure can be obtained directly from Eq.(A31):

$$\alpha_a = \sigma_a N_L \ell p_o \exp[-(\sigma_c + \sigma_j) N_L \ell p_o] . \quad (\text{A34})$$

The target gas pressure which provides maximum relative detectable current for the σ_a -transition can be determined by differentiating Eq.(A34) with respect to the reduced pressure and setting the result equal to zero, which yields

$$p_o \alpha_{am} = \frac{1}{(\sigma_c + \sigma_j) N_L \ell} . \quad (\text{A35})$$

Interpretation errors may result if the energy loss corresponding to one partial beam should coincide (within the limit of resolution of the apparatus) with the energy loss of another. The model portraying the superposition of two singly-scattered partial beams is shown in Fig. A4, where

$$\sigma_j'' = \sigma_j - \sigma_a - \sigma_b . \quad (\text{A36})$$

The solution for this model with the appropriate boundary

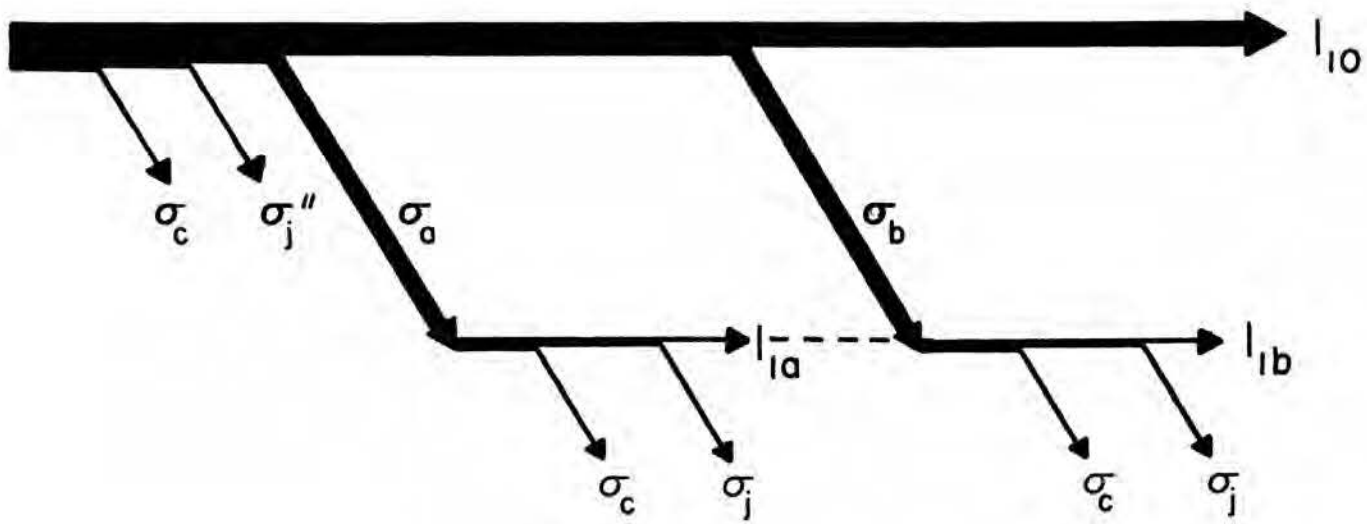


Fig. A4. Simplified partial beam model for two coincident singly-scattered beams.

conditions is

$$(I_{1a})_f + (I_{1b})_f = (I_{10})_i (\sigma_a + \sigma_b) n \ell \exp[-(\sigma_c + \sigma_j) n \ell] \quad (\text{A37})$$

or, with Eq.(A30),

$$\beta_a + \beta_b = \frac{(I_{1a})_f + (I_{1b})_f}{(I_{10})_f} \quad (\text{A38})$$

where

$$\beta_a = \sigma_a n \ell, \text{ etc.} \quad (\text{A39})$$

The result in Eq.(A38) describes precisely the situation where a discrete transition is superimposed on a continuum, such as that introduced by the $\Sigma\sigma(00/1_k q_\ell)$ interactions. Due to the additive, uncoupled nature of the results in Eq.(A38), the continuum in the energy-loss spectrum can be suppressed, exposing the isolated, discrete transition for evaluation.

Another interpretation error may occur if the energy-loss beam resulting from two successive inelastic collisions (double scattering) should coincide with that of a singly-scattered partial beam. The model describing this situation is shown in Fig. A5, where

$$\sigma_j''' = \sigma_j - \sigma_d . \quad (\text{A40})$$

The solution for this model is

$$\beta_a + \frac{\beta_b \beta_d}{2} = \frac{(I_{1a})_f + (I_{1,b+d})_f}{(I_{10})_f} . \quad (\text{A41})$$

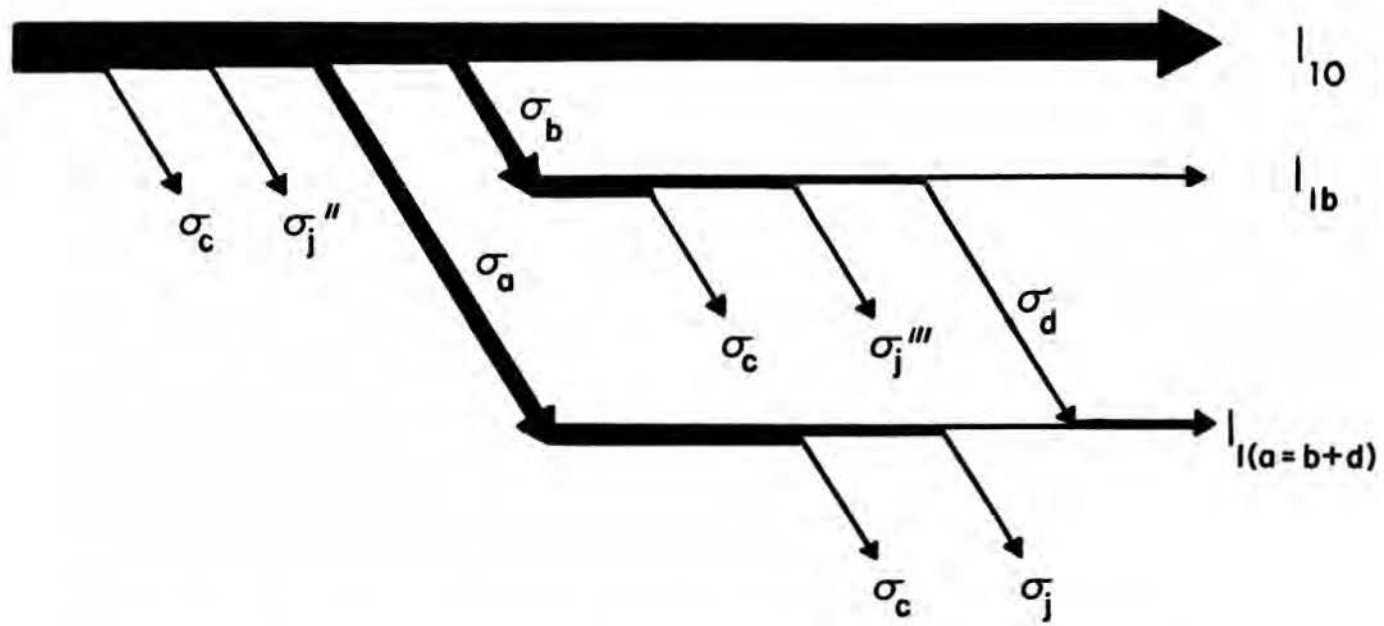


Fig. A5. Simplified partial beam model for coincident singly-scattered and doubly-scattered beams.

σ_b and σ_d can represent either identical, or entirely different, energy-loss transitions in the target particles.

In Eq.(A41), the relative doubly-scattered partial beam current is

$$\frac{(I_{1,b+d})_f}{(I_{10})_f} = \frac{\beta_b \beta_d}{2} \quad (\text{A42})$$

$$= \frac{1}{2} N_L^2 \lambda^2 p_0^2 \sigma_b \sigma_d \quad (\text{A43})$$

which varies quadratically with the reduced pressure. Least-squares fitting of experimental data can be used to isolate the square-law dependency of the double-scattering from the linear dependency of the single scattering. The latter can then be used for cross-section evaluation.

B. Least-Squares Fitting of Experimental Data

Least-squares fitting of experimental data for $(I_{1p})_f / (I_{10})_f$ versus reduced pressure to an equation of the form

$$\frac{(I_{1p})_f}{(I_{10})_f} = y = ap_o + bp_o^2 \quad (\text{B1})$$

yields

$$a = \frac{f_1}{\Delta} \quad (\text{B2})$$

and

$$b = \frac{f_2}{\Delta} \quad (\text{B3})$$

where

$$f_1 = \sum p_{on} y_n \sum p_{on}^4 - \sum p_{on}^2 y_n \sum p_{on}^3 \quad (\text{B4})$$

$$f_2 = \sum p_{on}^2 y_n \sum p_{on}^2 - \sum p_{on} y_n \sum p_{on}^3 \quad (\text{B5})$$

and

$$\Delta = \sum p_{on}^2 \sum p_{on}^4 - (\sum p_{on}^3)^2 \quad (\text{B6})$$

From Eq. (12),

$$a = \sigma_p N_L^\ell \quad (\text{B7})$$

$$b = \frac{\sigma_p N_L^{2\ell} \lambda}{2} = \frac{aN_L^{\ell\lambda}}{2} \quad (\text{B8})$$

The σ_p ionic-transition cross section, in this approximation, can be determined from Eq.(B7)

$$\sigma_p = \frac{a}{N_L \lambda} (1 + \epsilon_p) \quad (\text{B9})$$

where

$$\epsilon_p = \frac{s_a}{a} . \quad (\text{B10})$$

In Eq.(B10),

$$s_a = \left[\frac{\Sigma p_{on}^4 \Sigma (\delta y_n)^2}{(k - 2) \Delta} \right]^{1/2} \quad (\text{B11})$$

where

$$\begin{aligned} \Sigma (\delta y_n)^2 = \Sigma y_n^2 + a^2 \Sigma p_{on}^2 + b^2 \Sigma p_{on}^4 - 2a \Sigma p_{on} y_n \\ - 2b \Sigma p_{on}^2 y_n + 2ab \Sigma p_{on}^3 . \end{aligned} \quad (\text{B12})$$

Also, letting

$$z = \ln \left[\frac{(I_{10})_f}{(I_{10})_i} \right] \quad (\text{B13})$$

and least-squares fitting z versus reduced pressure to an equation of the form

$$z = - cp_o \quad (\text{B14})$$

yields

$$c = \frac{-\Sigma p_{on} z_n}{\Sigma p_{on}^2} . \quad (\text{B15})$$

From Eq.(A30),

$$c = (\sigma_c + \sigma_j) N_L \ell \quad (\text{B16})$$

which gives the total loss cross section for the incident beam

$$\sigma_c + \sigma_j = \frac{c}{N_L \ell} (1 \pm \epsilon_{cj}) \quad (\text{B17})$$

where

$$\epsilon_{cj} = \frac{s_c}{c} . \quad (\text{B18})$$

In Eq.(B18),

$$s_c = \left[\frac{\Sigma (\delta z_n)^2}{(k - 1) \Sigma p_{on}^2} \right]^{1/2} \quad (\text{B19})$$

where

$$\Sigma (\delta z_n)^2 = \Sigma z_n^2 + c^2 \Sigma p_{on}^2 + 2c \Sigma p_{on} z_n . \quad (\text{B20})$$

The relative change of the total loss cross section due to the projectile being excited through the σ_p -interaction can similarly be determined. Combining Eqs.(6), (B8) and (B16),

$$\zeta \equiv \frac{(\sigma_c + \sigma_j) - (\sigma_{ce} + \sigma_{je})}{\sigma_c + \sigma_j} = \frac{2b}{ac} (1 \pm \epsilon_\zeta) \quad (\text{B21})$$

where

$$\epsilon_\zeta = \left[\left(\frac{s_a}{a} \right)^2 + \left(\frac{s_b}{b} \right)^2 + \left(\frac{s_c}{c} \right)^2 \right]^{1/2} \quad (\text{B22})$$

and

$$s_b = \left[\frac{\sum p_{on}^2 \sum (\delta y_n^2)}{(k-2)\Delta} \right]^{1/2} . \quad (\text{B23})$$

C. Apparatus Modifications

The apparatus modifications which led to the improvement in resolution (0.6 - 0.8 eV FWHM) used in performing this study were principally as follows:

a) Significant reduction in magnitude of the transverse electrical fields applied to the beam. This was accomplished by rigidly mounting the scattering chamber on a two-axis gimbaled platform, which permitted precision angular and translational alignment of the scattering chamber defining orifices with the incident beam. In addition, all power supplies for the various sets of deflection plates were redesigned to provide "center-ground" configurations. With these alterations, the need for an angular deflection capability, previously required for beam navigation of the scattering chamber defining orifices, was completely eliminated.

b) Enhancement of analyzer resolution. This was accomplished by replacing the two fixed-width (0.013 cm) analyzer defining slits with externally manipulatable slits which were independently and continuously adjustable from zero to approximately 0.15 cm. Resolution was further increased by mounting the analyzer on a two-axis gimbaled platform which permitted precision alignment with the beam. Overall analyzer performance was improved by installing a new particle-multiplier tube having higher gain characteristics, by placing a conductive shield around the leading dynodes of the

tube, by trajecting the various electrical connections through individual vacuum feedthroughs in the analyzer walls rather than through a single octal feedthrough, and by installing a defining orifice in the analyzer which prevented peripheral beam ions from being detected by circumnavigating the slits.

c) Improvement of accelerator performance. This was accomplished largely through enhancing the decelerator alignment capability by installing an iris diaphragm and Faraday cup at each end of the deceleration column. The minimum 0.12 cm-diam openings permitted accurate alignment of the deceleration-column axis with the beam. Also, a fused-quartz disk was attached to the inner surface of the glass window on the straight-through magnet port. This permitted comparison of the optical location of the ion-source exit port, as viewed through the 0.051 cm-diam orifices of the scattering chamber, with the electrical location of the beam collimated by these two orifices, as indicated by the luminescence produced where the energetic beam struck the surface of the fused quartz. The chamber apertures, which originally were made of 0.025-cm sheet stainless steel and which had gradually tapering orifices, were replaced with 0.051-cm sheet tantalum (an anti-sputtering material) apertures having 45°-beveled orifices. The use of thicker material plus more steeply beveled orifices enhanced the conduction of heat away from the vicinity of the orifice, thereby considerably extending the useful lifetime

of these apertures. Operational control and stability were improved by modifying the existing Einzel-lens power connections to permit independent operation of the extractor and focus elements of the lens. Corona to the Einzel-lens high-voltage connections was minimized through oil-submersion of the associated resistor strings.

d) Reduction of residual background noise. This was accomplished by employing improved vacuum techniques. These improvements included replacing three 5.08 cm-diam copper-tubing slip joints with flexible bellows, enlarging the various vacuum openings in the analyzer to improve pumping efficiency, modifying existing Faraday cups to minimize residual leakage, and rigidly attaching the differential vacuum connections of the scattering chamber (this involved mounting a 15.24 cm-diam diffusion pump directly onto the gimballed platform). These improvements were realized in residual pressure reduction by almost an order of magnitude in some regions of the accelerator, permitting examination of spectra for fine detail with amplifications up to 10^5 over that required for the elastically scattered peak.

e) Enhancement of the reliability, stability, and accuracy of the target-gas pressure regulation. This was accomplished with pronounced shortening of all plumbing associated with the servo leak valve and the Baratron pressure head. The remaining plumbing, which previously consisted largely of 0.635 cm-diam tubing, was replaced almost

entirely with 1.270 cm-diam tubing. A stainless steel ballast tank installed in the gas-inlet system permitted operating with a smaller pressure gradient across the servo-leak valve. Due to the various improvements listed and due to the complications inherent in McLeod gauge application,^{33,34} the Baratron was taken as the laboratory pressure standard in preference to a McLeod gauge.

VII. BIBLIOGRAPHY

1. D. R. Bates, in Atomic and Molecular Processes (Academic Press, New York, 1962), p. 549.
2. J. T. Park and F. D. Schowengerdt, Rev. Sci. Instr. 40, 753 (1969).
3. J. T. Park and F. D. Schowengerdt, Phys. Rev. 185, 152 (1969).
4. F. D. Schowengerdt and J. T. Park, Phys. Rev. A1, 848 (1970).
5. J. Boudon, M. Barat, and M. Abignoli, J. Phys. B1, 1083 (1968).
6. D. F. Dance, M. F. A. Harrison, and A. C. H. Smith, Proc. Roy. Soc. (London) A290, 74 (1966).
7. E. J. R. Maier, J. Geophys. Res. 74, 815 (1969).
8. S. J. Bame, A. J. Hundhausen, J. R. Asbridge, and I. B. Strong, Phys. Rev. Letters 20, 393 (1968).
9. B. B. Jones, F. F. Freeman, and R. Wilson, Nature 219, 252 (1968).
10. H. Zirin and L. W. Acton, Astrophys. J. 148, 501 (1967).
11. W. L. W. Sargent and L. Searle, Astrophys. J. 152, 443 (1968).
12. C. Lari and G. Setti, Nuovo Cimento B52, 507 (1967).
13. E. W. McDaniel, Collision Phenomena in Ionized Gases (John Wiley and Sons, Inc., New York, 1964), p. 284.
14. H. S. W. Massey and R. A. Smith, Proc. Roy. Soc. (London) A142, 142 (1933).

15. Q. C. Kessel and E. Everhart, Phys. Rev. 146, 1524 (1965).
16. V. V. Afrosimov, Yu Gordiev, M. Panov, and
N. V. Fedorenko, Soviet Phys.-Tech. Phys. 11, 89 (1966).
17. M. Barat and J. C. Houver, Compt. Rend. 264B, 38, 296
(1967).
18. For a detailed discussion, see F. D. Schowengerdt, Ph.D.
dissertation, University of Missouri - Rolla (1969).
19. D. R. Schoonover, Ph.D. dissertation, University of
Missouri - Rolla (1970).
20. The procedure for least-squares fitting experimental data
to a mathematical function is given by Yardley Beers,
Introduction to the Theory of Error (Addison-Wesley Pub.
Co., Inc., 1957), pp. 38-43.
21. Colutron Corporation, Boulder, Colorado.
22. MKS Instruments, Inc., Burlington, Massachusetts.
23. J. Arol Simpson, G. E. Chamberlain, and S. R. Mielczardk,
Phys. Rev. 139, A1039 (1965).
24. V. I. Ochkur and A. M. Petrunkin, Opt. Spectry. (USSR)
14, 245 (1963).
25. D. F. Dance, M. F. A. Harrison, and A. C. H. Smith,
Proc. Roy. Soc. (London) A290, 74 (1966).
26. See, for example, H. R. Moustafa Moussa and F. J. DeHeer,
Physica 36, 646 (1967).
27. M. R. C. McDowell, NBS Tech. Note 185 (1963).
28. E. W. McDaniel, Collision Phenomena in Ionized Gases
(John Wiley and Sons, Inc., New York, 1964), p. 10.

29. D. W. Martin, R. A. Langley, D. S. Harmer, J. W. Hooper, and E. W. McDaniel, Phys. Rev. 136, A385 (1964).
30. S. K. Allison, Rev. Mod. Phys. 30, 1137 (1958).
31. B. M. Smirnov and M. I. Chivisov, Soviet Phys.-Tech. Phys. 10, 88 (1965).
32. E. S. Solov'ev, R. N. Il'in, V. A. Oparin, and N. V. Fedorenko, Soviet Phys.-JETP 18, 342 (1964).
33. Ch. Meinke and G. Reich, Vacuum 13, 579 (1963).
34. H. Ishii and K. Nakayama, Trans. 8th Vac. Symp. and 2nd Int'l. Congress (Pergamon Press, New York, 1962), pp. 519-524.

VIII. VITA

Donald Roy Schoonover was born near Pollock, Missouri on August 31, 1939. He received his elementary education from Pollock Grade School and his secondary education from Milan High School, graduating in 1957. After working at various jobs for a few years, he started to college in September, 1960. He subsequently received an Associate of Science degree in Engineering from the Junior College of Kansas City in June, 1962, a Bachelor of Science degree in Physics from the Missouri School of Mines and Metallurgy in May, 1964, and a Master of Science degree in Physics from the University of Missouri at Rolla in August, 1964. After working in the defense and aerospace industries near Los Angeles for a few years, he returned to complete his education in July, 1968.

He is married to the former Karen Clay of Green City, Missouri. They have one son, Donald Ray.